Journal of Molecular Liquids 355 (2022) 118948

Contents lists available at ScienceDirect

Journal of Molecular Liquids

journal homepage: www.elsevier.com/locate/molliq

Pore-scale simulation of nanoparticle transport and deposition in a microchannel using a Lagrangian approach

Milad Ramezanpour [a], Majid Siavashi [a,*], Ali Q. Raeini [b], Martin J. Blunt [b]

[a] Applied Multi-Phase Fluid Dynamics Laboratory, Iran University of Science and Technology, Tehran, Iran
[b] Department of Earth Science and Engineering, Imperial College London, London, United Kingdom

ARTICLE INFO

Article history:
Received 30 January 2022
Revised 10 March 2022
Accepted 14 March 2022
Available online 17 March 2022

Keywords:
Nanoparticle
Lagrangian
Van der Waals
Electrostatic
Brownian motion
Deposition

ABSTRACT

The application of nanoparticles to a fluid improves heat transfer and hydrodynamics, especially in porous media. To analyze the flow of nanoparticles and heat transfer in porous media at the pore scale, simulation in micro-scale channels of porous media is necessary. One concern is the deposition of nanoparticles to solid surfaces, which reduces the amount of material available in the bulk fluid. Also, in porous media, the nanoparticle deposition increases the surface roughness of pore surfaces, affecting the volumetric flow rate of nanofluid. Nanoparticle transport and deposition in a microchannel (as a representation of pore) are investigated numerically. The open-source library of OpenFOAM is used, and the Eulerian-Lagrangian (EL) approach is employed to simulate nanoparticles interacting with the base fluid and the surfaces of the microchannel. Integration of all forces exerted on nanoparticles, from base fluid and also microchannel's surfaces are considered simultaneously. Brownian motion, drag, buoyancy, gravity, and Saffman lift forces are considered between nanoparticles and the base fluid. Van der Waals and electrostatic double-layer forces based on DLVO theory are considered between nanoparticles and microchannel surfaces. The deposition ratio of nanoparticles (the fraction of nanoparticles that deposit on the solid surface) is analyzed by the variation of nanoparticle diameter, fluid velocity, temperature, surface potentials, and double-layer thickness. It is assumed that the nanofluid is dilute, and the collisions between the nanoparticles are neglected.

The results of nanoparticle deposition ratio are validated through comparison with available data in the literature. It has been shown that the nanoparticle deposition ratio decreases from 0.98 to 0.4 when the nanoparticle diameter increases from 30 to 150 nm. The effect of Van der Waals force on the enhancement of nanoparticle deposition ratio is about 1.6 %. Next, the deposition of nanoparticles is studied for different Reynolds number values, surface potential, nanoparticle radius, and double-layer thickness. Brownian motion dominates the behavior; increasing temperature and decreasing nanoparticle diameter will increase nanoparticle deposition. The magnitude of the nanoparticle and surface potentials and the double layer thickness are the two essential parameters that control the electrostatic double-layer force; its effect on deposition is also investigated. It has been concluded that the rise of the surface potential value decreases the deposition ratio.

1. Introduction

A nanofluid is the suspension of particles of size less than 100 nm in a liquid [1]. Over the years, nanotechnology has been used as an efficient tool in various engineering fields, and many experimental and numerical studies have been performed on different applications of nanofluids. The properties of nanoparticles are significantly different from those of larger particles because the fraction of atoms on the particle's surface increases as it reaches the nanometer dimension. Also, nanoparticles have a high surface-to-volume ratio, leading to a wide range of nanofluid applications, such as energy devices, solar systems, the automotive industry, and enhanced oil recovery [2]. Some applications of nanofluids are shown in Fig. 1.

One of the applications of nanofluids is the enhancement of cooling or heating functions in energy devices [3-5]. By introducing nanoparticles into the liquid, the heat transfer properties of the

* Corresponding author at: School of Mechanical Engineering, Iran University of Science and Technology, Narmak, Tehran Postal Code: 1684613114, Iran.
E-mail addresses: m_ramezanpour@mecheng.iust.ac.ir (M. Ramezanpour), msiavashi@iust.ac.ir (M. Siavashi), a.q.raeini@gmail.com (A.Q. Raeini), m.blunt@imperial.ac.uk (M.J. Blunt).

https://doi.org/10.1016/j.molliq.2022.118948
0167-7322/

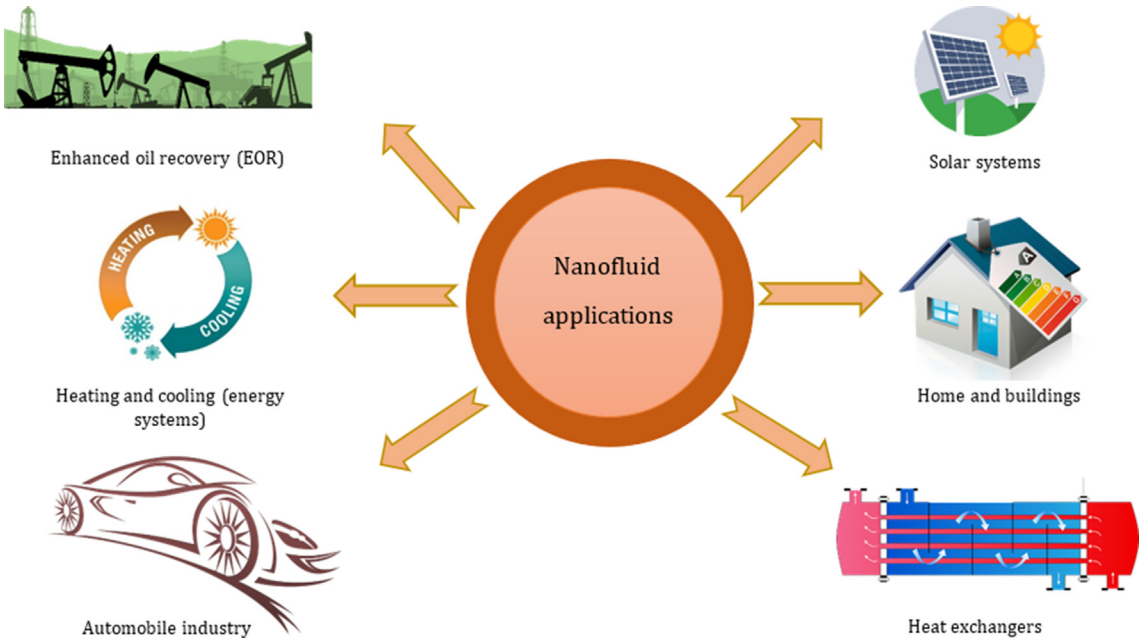

Fig. 1. Some common applications of nanofluids.

nanofluid are improved compared to the pure fluid, which increases the system's efficiency [6]. For instance, nanofluids are commonly used in cooling systems [7,8]. It has been shown experimentally that the existence of ZnO nanoparticles in different concentrations in the base fluid increases the heat transfer characteristics of an automobile radiator compared to the pure fluid [9]. In addition, for the same reasons, nanofluids are used in circular tube heat exchangers [10], plate heat exchangers [11], shell and tube heat exchangers [12], and also in tube and pipes [13,14]. Due to nanofluid's function in enhancing heat transfer, numerical studies are of interest in the literature [15,16]. For instance, in a study by Rostami et al. [17], an artificial neural network (ANN) was developed and used to predict the thermal conductivity of multi-walled carbon nanotubes-CuO/water nanofluid. In another study, ANN was used to predict the viscosity of Silver/Ethylene glycol nanofluid at different temperatures and volume fractions of nanoparticles [18].

Solar thermal collectors act as heat exchangers to transform the energy from solar radiation into the internal energy of the transport medium [19]. Enhancing the performance of solar systems with nanofluids due to their high thermal conductivity compared to a pure fluid is another application of nanofluids. In a study by Said et al. [20], carbon nanotubes-based nanofluids as an absorbing medium were used to evaluate the increase in heat transfer, entropy generation, and pressure drop in a flat-plate solar collector. Using carbon and metal oxide-based nanoparticles in a flat-plate solar collector was experimentally investigated by Akram et al. [21]. The use of single-walled carbon nanohorn-water nanofluid as the working fluid in a direct absorption solar collector and porous receiver accompanied by nanoparticle addition to working fluid in a parabolic solar collector were studied by Siavashi et al. [22,23]. It has been shown that by increasing the nanoparticle volume fraction to 0.015 in nanofluid, the thermal efficiency increases 12%. To enhance the thermal energy storages in solar systems, the numerical approach was used in a study by Bhatti et al. [24]. They investigated the unsteady flow confined by parallel rotating plates in the porous media with nanofluid. They concluded that the temperature distribution increases with the rise of Brownian and thermophoretic forces parameters.

Nanofluid flow in porous media is also of interest in the literature [25-28]. One of the applications of nanofluid in porous media is related to the petroleum industry for enhanced oil recovery (EOR) [29,30]. Nanofluids can reduce the interfacial tension between oil and water, which aids the displacement of oil from the pore space [31]. Wettability and viscosity alteration [32,33] can also enhance oil recovery. In recent years, researchers have conducted various laboratory and numerical studies on nanofluid flooding in EOR [19,20]. It has been concluded that flooding of engineered carbon nanosheets in brine with only 0.1 wt% resulted in incremental oil production of 20% [34].

One concern in all these applications is the deposition of nanoparticles to the solid surfaces of the device. This removes particles from the bulk fluid, reducing the efficiency and effectiveness of heat transport or other processes and clogging of flow channels. In addition to the importance of particle deposition in industrial applications, this issue is also crucial in the subjects related to human health [35].

Nanoparticle transport and deposition in porous media depend on events that occur on the pore scale. Colloid filtration theory (CFT) is the most common model to predict particles' retention coefficient on the surface for a wide range of conditions [36]. In this method, the contact efficiency of spherical collectors as a porous medium saturated by the base fluid is determined by a mechanical approach that traces the nanoparticle trajectories. The calculated contact efficiency in the continuum method is upscaled into the kinetic retention coefficient [37]. Chatterjee and Gupta [38] developed a model based on colloid filtration theory which accounts for the possibility of aggregation of the particles. The agglomeration of particles of different sizes was studied in this model. In another study on CFT, Molnar et al. [39] investigated the retention and transport of nanoparticles in porous media by employing X-ray computed microtomography. In the study of Molnar et al. [39], it was determined that silver nanoparticle concentrations are significantly lower near grain-grain contacts.

Despite the extensive studies in CFT, this approach has some limitations, principally the simplification of the porous medium to equivalent collectors. Hence, other methods based on direct simulation to study the transport and deposition of nanoparticles in

porous media have been considered in recent years. Eulerian-Eulerian (EE) and Eulerian-Lagrangian (EL) numerical approaches are used in the literature to simulate nanoparticle transport in porous media and microchannels. In the EE approach, continuity and momentum equations are solved to simulate the fluid flow and nanoparticle transport as separate phases. The volume-of-fluid (VOF), mixture, and Eulerian models are the main methods in the EE approach [40]. Eulerian models can be used for dense fluids in which the concentration of nanoparticles is such that the nanoparticles can be considered as a continuous phase. However, the EL approach is used for dilute nanofluids to investigate the nanoparticle transport and fluid flow simulation. The Navier-Stokes equations are solved for fluid flow in the EL approach, and Lagrangian particle tracking is employed to model nanoparticle transport. The EL approach is more accurate than the EE approach, but its computational cost is higher [40].

The utilization of the Lagrangian approach to study particle deposition in the microchannel is of interest in the Literature [41]. Ghafouri et al. [42] used the Lagrangian approach to investigate the deposition and dispersion of micro-scale particles over the triangular cylinders in a two-dimensional channel. The effect of Brownian, gravity, Saffman and Drag forces were also considered between particles and fluid. They concluded that particle deposition enhances with the rise of fluid velocity.

In a numerical study by Malvandi et al. [43], the thermal performance of an alumina-water nanofluid in a circular microchannel was investigated. The flow was assumed to be fully developed, and Buongiorno's model [44], considering Brownian motion and thermophoresis forces, was employed to solve the flow. In another work by Malvandi et al. [45] using the previously-mentioned model, nanoparticle migration was considered to study the transport phenomena of titania-water and alumina-water in a condensation film.

In another study, the forced convection flow of alumina-water nanofluid in a two-dimensional baffled flow was numerically investigated by Fazeli et al. [46]. The Navier-Stokes and nanofluid transfer equations were solved by considering Brownian motion and thermophoresis forces. The effects of nanoparticle concentration, Reynolds number, and nanoparticle diameter on the heat transfer coefficient, nanoparticle distribution, velocity, and temperature fields were investigated.

Nanoparticle transport and deposition in a microchannel to represent pore-scale phenomena was simulated by Seetha et al. [47]. It was assumed that fluid flow was fully developed, and the advection–diffusion equation was solved for nanoparticle transport. The effects of Brownian diffusion, electrostatic double layers, and Van der Waals forces were also considered. The deposition of nanoparticles was influenced by the variation of nanoparticle diameter, pore channel width, and the parameters related to the forces between the nanofluid and surface walls, such as surface potentials and double layer thickness.

Nanoparticle transport and deposition were also investigated in various numerical studies by the EL approach. Heat transfer and dispersion of nanoparticles in a microchannel were studied by Nayinian et al. [48]. The effects of drag, Saffman lift, Brownian motion, and gravitation forces are included in the Lagrangian part of the equation. The working fluid was assumed to be air under a slip flow regime. An analytical method was also used to determine nanofluid flow in a microchannel by Afshar et al. [49]. In addition, nanoparticle transport in a microchannel considering near-wall corrections was studied numerically by Andarwa et al. [50,51]. The lattice Boltzmann method coupled with Lagrangian particle tracking was solved to investigate nanoparticle deposition. The effect of pressure gradient and nanoparticle diameter considering Saffman lift, drag, Brownian motion, gravitational, and Van der Waals forces were investigated in that study. In another study, Sharaf et al. [37] used a two-way coupling EL approach to investigate nanoparticle migration and convective heat transfer in a microchannel. The effect of Brownian and thermophoresis forces on the deposition ratio of nanoparticles on microchannel surfaces was also investigated.

In a study, the nanoparticle deposition for flow through a channel with a constant heat flux was investigated numerically [52]. The Lagrangian approach was used in that study. The effects of porous permeability, Reynolds number, volume concentration, and different particle forces on particle deposition were studied. The effects of drag, Brownian, thermophoresis, gravity, and Van der Waals forces were considered in that study.

In these previous studies, the behavior of nanoparticles in a microchannel or porous medium was investigated by considering the different forces at play. Some research concentrated on the forces between nanoparticles and fluid, including Brownian motion or thermophoretic forces. Other studies have focused on the behavior of nanoparticles in interaction with the wall surfaces (a summary of some of the published papers in the literature is listed in Table 1). However, a complete study of the effect of all forces affecting the deposition of nanoparticles on the surface has not been addressed comprehensively. Hence, it is essential to study the deposition of nanoparticles on the surfaces of porous media. It is necessary to provide a mathematical model that can integrate the effects of different forces, including the forces between nanoparticles and base fluid, and between nanoparticles and the wall surfaces, which is lacking from previous studies.

Using the OpenFOAM finite open-source library, a numerical solver is developed to investigate nanoparticle transport and deposition in microchannels. Due to the dominant effect of Brownian motion on nanoparticle deposition, the impact of this effect is considered in this study. Moreover, drag, buoyancy, gravity, and Saffman lift forces are considered between nanoparticles and the base fluid. In addition to the forces between the nanoparticles and the fluid, Van der Waals and electrostatic double-layer forces between the nanoparticles and the microchannel surfaces based on DLVO theory are also accounted for. The deposition of nanoparticles is studied for different values of four parameters: Reynolds number, magnitudes of the surface potentials, the ratio of nanoparticle radius to double layer thickness, and nanoparticle radius. Also,

Table 1
Summary of previous studies in the literature.

Authors	Approach and effective forces
Chatterjee and Gupta [38]	colloid filtration theory (CFT)
Molnar et al. [39]	colloid filtration theory (CFT)
Ghafouri et al. [42]	Lagrangian approach –micro-scale particles– Brownian, gravity, Saffman, and Drag forces
Malvandi et al. [43]	Buongiorno's model –nanofluid– Brownian motion and thermophoresis forces
Malvandi et al. [45]	Buongiorno's model –nanofluid– Brownian motion and thermophoresis forces
Fazeli et al. [46]	Eulerian –nanofluid– Brownian motion and thermophoresis forces
Seetha et al. [47]	Eulerian –nanofluid– Brownian diffusion, electrostatic double layers, and Van der Waals forces
Nayinian et al. [48]	Lagrangian –nanofluid– drag, Saffman lift, Brownian motion, and gravitation forces
Afshar et al. [49]	Eulerian –nanofluid– drag, Saffman lift, Brownian motion, and gravitation forces
Andarwa et al. [50,51]	Lagrangian –nanofluid– drag, Saffman lift, Brownian motion, gravitation, and Van der Waals forces
Sharaf et al. [37]	Lagrangian –nanofluid– drag, Saffman lift, Brownian motion, and gravitation forces
Albojamal and Vafai [52]	Lagrangian –nanofluid– drag, Brownian, thermophoresis, gravity, and Van der Waals forces

the effect of the temperature variation of the nanofluid mixture on particle deposition is examined.

2. Theoretical background

The EL approach is employed to simulate the nanoparticle behavior in interaction with the base fluid and microchannel surfaces. The following assumptions are made:

- The nanofluid is dilute, nanoparticles do not aggregate, and collisions between nanoparticles are neglected. Hence, a one-way coupling assumption is used, and the effects of nanoparticles on fluid flow are ignored.
- The temperature in the microchannel environment, including the surfaces and the fluid, is considered constant.

To simulate the transport and deposition of nanoparticles in the base fluid, a two-dimensional microchannel with a rectangular cross-section (with H as the height and L as the length of the microchannel) is used (see Fig. 2).

2.1. Governing equations

In the EL approach, the base fluid is considered continuous, and the continuity and momentum equations are solved for fluid flow [40]:

$$\nabla.\left(\rho_f \boldsymbol{U}_f\right) = 0 \tag{1}$$

$$\rho_f(\boldsymbol{U}_f.\nabla)\boldsymbol{U}_f = -\nabla \mathrm{p} + \nabla.\left[\mu_f\left(\nabla \boldsymbol{U}_f + \nabla \boldsymbol{U}_f{}^T\right)\right] + S_m \tag{2}$$

where ρ_f is the fluid density, μ_f is fluid viscosity, $\boldsymbol{U}_f$ is the fluid velocity, and S_m is the source term indicating the momentum transfer between the fluid and nanoparticles. S_m is calculated using [40]:

$$S_m = \frac{1}{\delta V}\sum_{p=1}^{n_p} m_p \boldsymbol{F}_p \tag{3}$$

The subscript p represents the particle, m_p and $\boldsymbol{F}_p$ indicate the particle's mass and the particle's total force on the fluid (per unit mass), respectively. δV is the computational cell volume, and n_p is the number of nanoparticles in a computational cell. The force between the particles and the fluid is the sum of all the forces between the particles and the fluid.

In this simulation, it has been assumed that the fluid flow is fully developed, and the continuity and momentum equations can lead to the following analytical solution to present the velocity profile [49]:

$$\boldsymbol{U}_f = \frac{H^2}{8\mu}\left(-\frac{dp}{dx}\right)\left(1 - \left(\frac{2y}{H}\right)^2 + 8\frac{2-\sigma}{\sigma}Kn_{ch}\right) \tag{4}$$

in which H is the height of the microchannel, y is the distance from the channel centerline,σ is the tangential momentum accommodation coefficient and is assumed to be 1, and $Kn_{ch} = \lambda/H$ is the channel's Knudsen number [49,50].

Newton's law for nanoparticle transport in the Lagrangian method is [40]:

$$m_p \frac{d\boldsymbol{U}_p}{dt} = \boldsymbol{F}_p \tag{5}$$

As mentioned above, $\boldsymbol{F}_p$ in Eq. (5) is the sum of the forces between the nanoparticles and the fluid. In addition to the forces between nanoparticles and fluid, interparticle forces and the forces between nanoparticles and the wall are also affect the behavior.

As previously mentioned, the effect of interparticle forces and the collision of nanoparticles are neglected due to the low concentration of the nanofluid. Hence, only the forces between the nanoparticles and the fluid and the nanoparticles and the wall are considered. Therefore, Eq. (5) can be rewritten by considering drag, Brownian, Saffman lift, buoyancy, and gravity as the most dominant forces between the base fluid and nanoparticles. Besides, Van der Waals (VDW) and electrostatic double layer (EDL) forces are accounted as the forces between microchannel surface and nanoparticles, and Eq. (5) is written as follows [40,50,51]:

$$\begin{aligned} m_p \frac{d\boldsymbol{U}_p}{dt} &= \boldsymbol{F}_p \\ &= \boldsymbol{F}_{Drag} + \boldsymbol{F}_{Brownian} + \boldsymbol{F}_{Saffman} + \boldsymbol{F}_{Bouyancy} + \boldsymbol{F}_{Gravity} + \boldsymbol{F}_{VDW} \\ &\quad + \boldsymbol{F}_{EDL} \end{aligned} \tag{6}$$

2.1.1. Drag force

Due to the relative motion between the nanoparticles and the fluid, the drag force is applied in the opposite direction of the nanoparticles' motion. The drag force is given by [50]:

$$\boldsymbol{F}_{Drag} = m\frac{18\mu_f}{\rho_p {d_p}^2 C_c}(\boldsymbol{U} - \boldsymbol{U}_p) \tag{7}$$

C_c is the Cunningham slip correction factor, and d_p is the nanoparticle diameter. When the particle radius decreases to the nanometer scale, the no-slip assumption is no longer valid. Hence, the drag force expression will be corrected with the Cunningham slip correction factor. Based on the empirical study of Kim et al. [53] on the calculation of Cunningham slip correction factor for temperatures in the range of 300 K, C_c is as follows:

$$C_c = 1 + \mathrm{Kn}\left(\alpha + \beta \exp\left(-\frac{\gamma}{Kn}\right)\right) \tag{8}$$

where α, β, and γ are 1.165, 0.483, 0.997, respectively. In the above equation, Kn is the Knudsen number, defined as the ratio of mean free path of base fluid molecules (λ) to the nanoparticle radius (r_p), $\mathrm{Kn} = \lambda/r_p$.

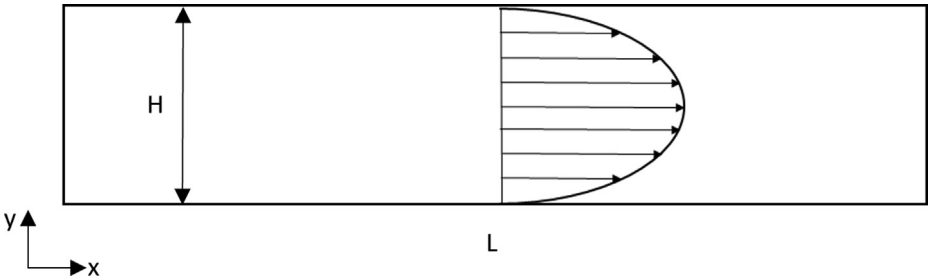

Fig. 2. A schematic representation of microchannel.

2.1.2. Brownian motion

As a result of the collision between the base fluid molecules and the particles, a Brownian force is created, which causes the random motion of particles. This force increases with decreasing particle size and, therefore, dominates the transport behavior.

Due to the random nature of the Brownian motion, it is modeled as a Gaussian white noise random process. The components of the Brownian force at each time step is calculated with the following relation [54]:

$$\boldsymbol{F}_{Brownian,i} = m_p \varsigma_i \sqrt{\frac{\pi S_0}{\Delta t}} \tag{9}$$

ς_i is the zero-mean, independent Gaussian random number with unit variance, Δt is the time-step, and S_0 is the spectral intensity given by [54]:

$$S_0 = \frac{216\mu_f k_b T}{\pi^2 {\rho_p}^2 {d_p}^5 C_c} \tag{10}$$

$k_b = 1.3806 \times 10^{-23} \mathrm{m^2 kg/(s^2 K)}$ is the Boltzmann constant, and T is the fluid temperature.

For the calculation of the Brownian motion, a procedure proposed by Abouali et al. [55] is used:

- Choose a time-step (Δt)
- Generate a sequence of uniform random numbers (A_i)
- Transform these random numbers to pairs of zero-mean Gaussian random numbers with unit variance:

$$\varsigma_1 = \sqrt{-2\ln(A_1)}\cos(2\pi A_2) \tag{11}$$

$$\varsigma_2 = \sqrt{-2\ln(A_1)}\sin(2\pi A_2) \tag{12}$$

- Calculation of Brownian force by Eqs. (9)–(12).

2.1.3. Saffman lift force

Tiny particles in a shear flow are subjected to a force perpendicular to their direction [56]. Saffman [57,58] proposed a relation for calculating this force, which is called the Saffman lift force:

$$\boldsymbol{F}_{Saffmann} = 6.46 {r_p}^2 (\boldsymbol{U} - \boldsymbol{U}_p) \sqrt{\rho\mu \left|\left(\frac{\partial \boldsymbol{U}}{\partial y}\right)\right|} \mathrm{Sign}\left(\frac{\partial \boldsymbol{U}}{\partial y}\right) \boldsymbol{e}_y \tag{13}$$

2.1.4. Buoyancy and gravity forces

The sum of gravity and buoyancy (obtained from Archimedes' law) forces is represented as [40]:

$$\boldsymbol{F}_{Bouyancy} + \boldsymbol{F}_{Gravity} = (\pi \frac{{d_p}^3}{6})\left(\rho_f - \rho_p\right)\boldsymbol{g} \tag{14}$$

2.1.5. Van der Waals (VDW) force

The interaction between nanoparticles and microchannel surfaces is significant at distances of a few nanometers. A theory was developed by Derjaguin, Landau, Verwey, and Overbeek to explain the stability of colloidal dispersion, which is called the DLVO theory [59,60]. Based on the DLVO theory, the VDW and EDL forces act as attractive and repulsive forces: how they are incorporated into the model is described below.

VDW is an attractive force between small particles and surfaces [59]. This force is significant at short distances between two surfaces from the atomic range to more than 10 nm [61]. The VDW force is only considered between nanoparticles and the microchannel surfaces [62]:

$$\boldsymbol{F}_{VDW} = \frac{A_H}{6}\left[-\frac{r_p}{(z-r_p)^2} - \frac{r_p}{(z+r_p)^2} + \frac{1}{z-r_p} - \frac{1}{z+r_p}\right] \tag{15}$$

where A_H is the Hammaker's constant for a spherical nanoparticle, and z is the nearest distance between the nanoparticle and the wall surface.

2.1.6. Electrostatic double layer (EDL) force

Due to the existence of ions in the base fluid, solid particles in a liquid with a high dielectric constant will be charged, and an electric double layer is created around the charged particles [60]. By the using of Hogg-Healy-Fuerstenau (HHF) formulae [63], the energy of electrostatic interaction between two different surfaces is as follows [60]:

$$\boldsymbol{E}_{EDL} = \pi\varepsilon\varepsilon_0 r_p ({\psi_1}^2 + {\psi_2}^2)\left[\frac{2\psi_1\psi_2}{{\psi_1}^2 + {\psi_2}^2}\ln\left(\frac{1+\exp(-\kappa z)}{1-\exp(-\kappa z)}\right) + \ln(1-\exp(-2\kappa z))\right] \tag{16}$$

The force of the electrostatic double layer is calculated as:

$$\boldsymbol{F}_{EDL} = \frac{-d\boldsymbol{E}_{EDL}}{dz} = 2\kappa\pi\varepsilon\varepsilon_0 r_p ({\psi_1}^2 + {\psi_2}^2)\left[\frac{\frac{2\psi_1\psi_2}{{\psi_1}^2+{\psi_2}^2} - \exp(-\kappa z)}{\exp(\kappa z) - \exp(-\kappa z)}\right] \tag{17}$$

where ψ_1 and ψ_2 are the nanoparticle and surface potentials, κ is the inverse of Debye-Huckel length, ε is the dielectric constant of the solution, and ε_0 is the permittivity of vacuum.

In the study of Rajagopalan and Kim [64], three dimensionless parameters are introduced for the calculation of electrostatic double layer force, which are:

$$\mathrm{N_{E1}} = \frac{\pi\varepsilon\varepsilon_0 r_p ({\psi_1}^2 + {\psi_2}^2)}{k_B T} \tag{18}$$

$$\mathrm{N_{E2}} = \frac{2\psi_1\psi_2}{{\psi_1}^2 + {\psi_2}^2} \tag{19}$$

$$\mathrm{N_{DL}} = \kappa r_p \tag{20}$$

Using Eqs. (18)–(20), Eq. (17) can be written:

$$\boldsymbol{F}_{EDL} = 2\kappa k_B T \mathrm{N_{E1}}\left[\frac{\mathrm{N_{E2}} - \exp(-\mathrm{N_{DL}} z^*)}{\exp(\mathrm{N_{DL}} z^*) - \exp(-\mathrm{N_{DL}} z^*)}\right] \tag{21}$$

where $z^* = \frac{z}{r_p}$. The physical properties of fluids and nanoparticles are listed in Table 2.

Table 2
The physical properties of nanoparticles and fluids.

Parameter	Value
The density of air, ρ_f	1.184 kg/m^3
The density of water, ρ_f	998.21 kg/m^3
The density of nanoparticle, ρ_p	7870 kg/m^3
The viscosity of air, μ_f	1.1849×10^{-5} kg/(m.s)
The viscosity of water, μ_f	1.002×10^{-3} kg/(m.s)
The characteristic wavelength of air, λ	67 nm
The characteristic wavelength of water, λ	100 nm
Hammaker constant for air, A_H	1×10^{-20}
Hammaker constant for water, A_H	0.4×10^{-20}
Boltzmann constant, k_B	1.38×10^{-23} J/K

2.2. Solver development

A numerical solver using the OpenFOAM finite open-source library is modified to model the transport and deposition of nanoparticles in a base fluid flowing in a microchannel. The finite volume method (FVM) is used to solve the equations of the fluid phase. This solver comprises the Lagrangian source code coupled with the PIMPLE algorithm to solve the Eulerian section. The Navier-Stokes equations and average volume continuity are solved with the PIMPLE algorithm. In this solver, through the calculation of momentum exchange and local particle volume fraction, the fluid velocity is calculated.

The discretization is performed by the second-order central difference scheme and first-order Euler scheme for the pressure gradient and time derivative, respectively [65]. A conjugate gradient solver solves the result of Eulerian discretized systems with geometric, algebraic multi-grid preconditioning for pressure and a smooth solver with Gauss-Seidel smoothing for velocity, which is available in OpenFOAM.

The code developed in this study can calculate all the forces introduced in the previous section between the base fluid and nanoparticles and between the wall surface of microchannel and nanoparticles.

The base fluid flow has been assumed to be fully developed (Eq. (4)). Hence, Lagrangian particle tracking is implemented in a one-way coupling method using the calculated flow field. The numerical solution process is as follows:

- The information of all nanoparticles is stored in a data structure.
- Velocities and positions of all nanoparticles are calculated and passed to the Eulerian section.
- The positions of all nanoparticles are determined within the Eulerian mesh.
- Nanoparticles' volume fractions are computed in each cell of Eulerian mesh.
- The forces acting on the nanoparticles –from the fluid and the wall– are calculated.
- The nanoparticle velocity field for the next time step is calculated.

3. Results and discussion

The deposition of nanoparticles on microchannel surfaces may lead to clogging with subsequent effects on flow and transport, as well as a loss of nanoparticles in the bulk fluid. When the distance of the center of spherical nanoparticles to the surfaces of microchannels is equal to or less than the nanoparticle radius, deposition occurs [50,66]. It has been assumed that the microchannel in this study is two-dimensional. Nanoparticles are randomly distributed in the inlet of the microchannel. They are injected with a constant velocity equal to 80 percent of the mean velocity of the fluid [50]. These particles can be escaped from the opposite microchannel surface (outlet) or deposited on the top and bottom surfaces. One thousand nanoparticles are injected into the microchannel. These conditions are kept constant for all simulations done in this study. In addition, some results are repeated for 2000, 3000, and 5000 nanoparticles. However, the difference in the results is negligible.

The results will be presented as the deposition ratio of nanoparticles in different circumstances in two sections. The nanoparticle deposition ratio is defined as the ratio of the number of deposited nanoparticles on the surface of microchannels to the number of injected nanoparticles. First, the deposition in the air is investigated. EDL is important in liquids like water, with a high dielectric constant [60] but of less importance for a gas. Hence, in this section, the effect of the EDL force is ignored [50]. In the second section, water is considered as the base fluid, and the effects of the EDL force are considered. The simulation time continues until the last nanoparticle leaves the microchannel or deposits on the microchannel surfaces. The range of physical parameters used in the simulation is listed in Table 3.

3.1. Validation

In this section, the microchannel height (H) is equal to 4 μm, and its length (L) is 1 mm. Fig. 3 shows the deposition ratio for four values of nanoparticle diameter: 30, 50, 100, and 150 nm. The simulation is performed with and without considering the VDW force. The attractive VDW force increases the amount of deposition from 0.5 to 1.6% for different nanoparticle diameters. As is stated in Eq. (10), the Brownian motion force is inversely proportional to d_p^5. Hence, due to the dominant effect of Brownian motion at the nanoscale, there is less deposition of larger particles.

Also, the results are validated with the study of Andarwa et al. [50]. As shown in Fig. 3, the difference between the values calculated in this study and the previous research is minimal. This slight difference could be caused by the difference in the number of injected nanoparticles in the microchannel and the difference in injection method. In this study, it has been assumed that all of the nanoparticles are injected randomly from the inlet of the microchannel in about 10^{-7} s.

3.2. Air as the base fluid

Transport and deposition of nanoparticles with a 30 and 150 nm diameter are indicated in Fig. 4 and Fig. 5, respectively. Due to the length of the microchannel, the size of nanoparticles is magnified by a factor of 7. The results are displayed at the microchannel inlet after 0.0002 s.

As shown in these figures, the nanoparticle deposition ratio on the microchannel surfaces at t = 0.0002 s for nanofluid with 30 nm nanoparticles is 0.6, which is higher than the nanofluid with 150 nm nanoparticles with a 0.19 deposition ratio.

The effect of pressure gradient on nanoparticle deposition ratio for four values of nanoparticle diameter is calculated and depicted in Fig. 6. Since the flow is fully developed, an increase in the pressure gradient simply increases the velocity of the fluid in proportion. As shown in this figure, the nanoparticle deposition ratio decreases with a rise of pressure gradient from 10 to 50 MPa/m. With an increase of fluid velocity, the Re number increases, and based on the definition of Peclet number Pe = Re.Sc, which indicates the ratio of advective transport to diffusive transport, this ratio increases. Hence the nanoparticle transport to the microchannel surfaces decreases, and the nanoparticle deposition ratio falls.

Brownian motion acts as the dominant interaction between particles and fluid on the nanoscale. Based on Eqs. (9), (10), increasing the temperature amplifies this effect. As exhibited in Fig. 7, when the temperature increases from 300 K to 600 K, the deposition ratio for nanoparticles with 50 nm diameter increases from 0.62 to about 0.83.

Table 3
The range of physical parameters used in the simulation.

Parameter	Value
Particle diameter,d_p	$30-150$ nm
Pressure gradient,$\frac{dp}{dx}$	$10-50$ MPa/m
Temperature,T	$300-600K$
particle radius to the double layer thickness ratio,N_{DL}	$1-100$
The magnitude of the surface potentials,N_{E1}	$1-150$
Reynolds number,Re	$1, 5,$ *and* 10

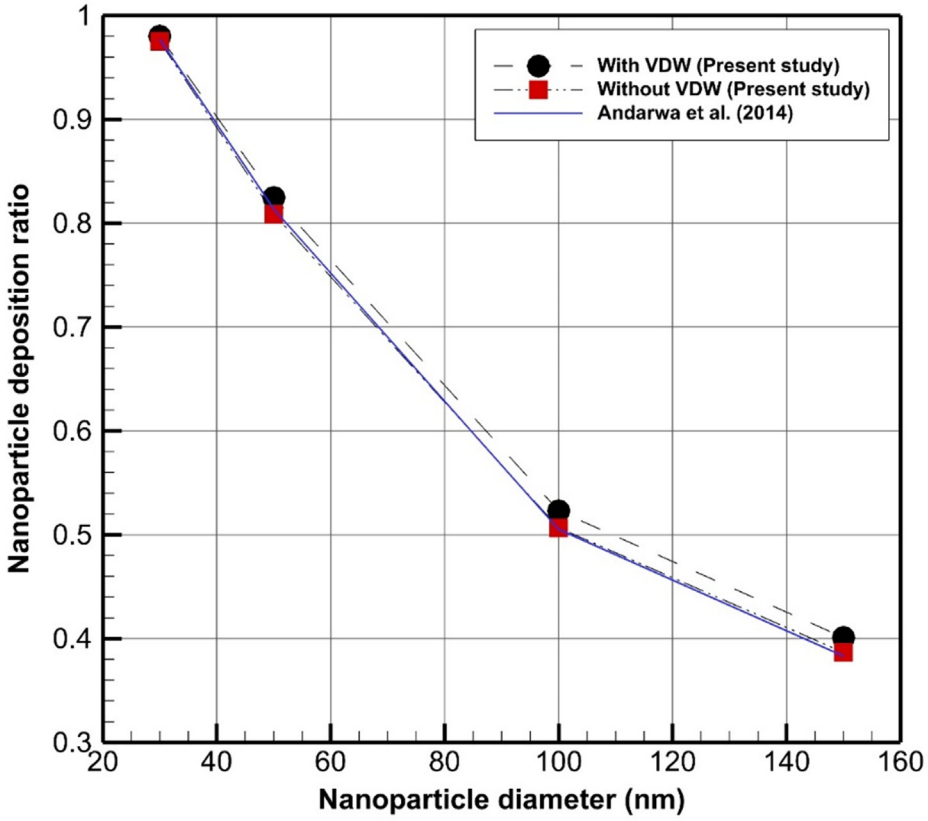

Fig. 3. Simulation results for the effect of VDW force on nanoparticle deposition ratio following through a microchannel for different values of nanoparticle diameter and comparison with results of Andarwa et al. [50].

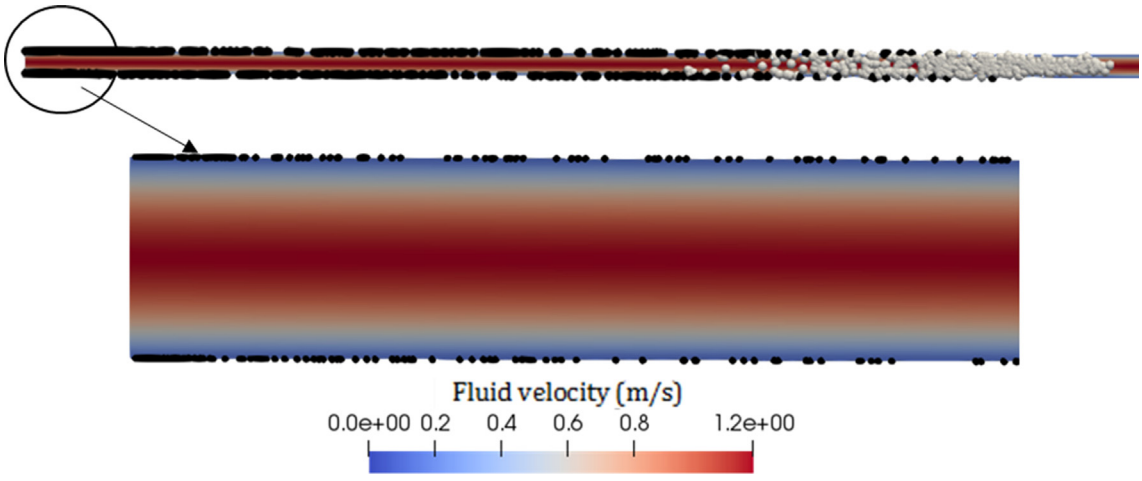

Fig. 4. Transport and deposition of nanoparticles with d_p = 30 nm at t = 0.0002 s (black nanoparticles are deposited on the surfaces).

The dominant effect of Brownian motion force on nanoparticle deposition is compatible with the data published in the literature. In a study by Albojamal and Vafai [52], it has been reported that the Brownian motion is the most dominant force with a 48% increasing effect in the relative deposition when individually omitted.

3.3. Nanoparticle transport in water

In this section, the height of the microchannel (H) is set to 10 μm, its length (L) is 250 μm, and water is used as the base fluid. Water has a high dielectric constant and is an explicit solvent for ions. Hence, the surfaces in water are mainly charged. Surface charges cause an electric field that attracts counter-ions. The layer composed of surface charges and ions is called the EDL, which is included in the analysis of this section [60].

In Fig. 8, the nanoparticle deposition ratio for different values of N_{E1} and N_{DL} is investigated. It has been assumed that the Reynolds number is 1, N_{E2}=1, and the radius is 15 nm for all injected nanoparticles. As mentioned in section 2.1.6, N_{E1} and N_{DL} are two non-dimensional parameters. N_{E1} represents the magnitude of the nanoparticle and microchannel surface potentials, and N_{DL}

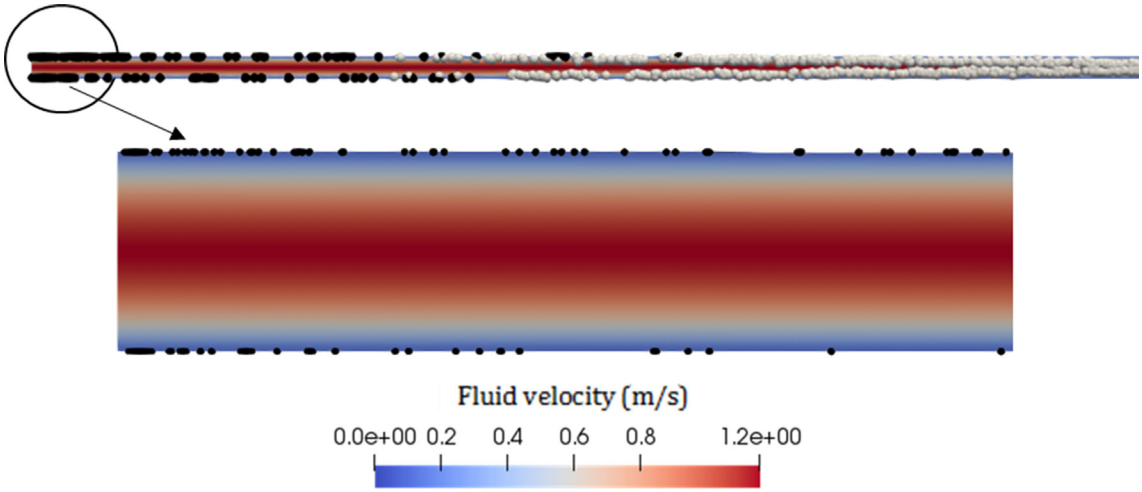

Fig. 5. Transport and deposition of nanoparticles with d_p = 150 nm at t = 0.0002 s (black nanoparticles are deposited on the surfaces).

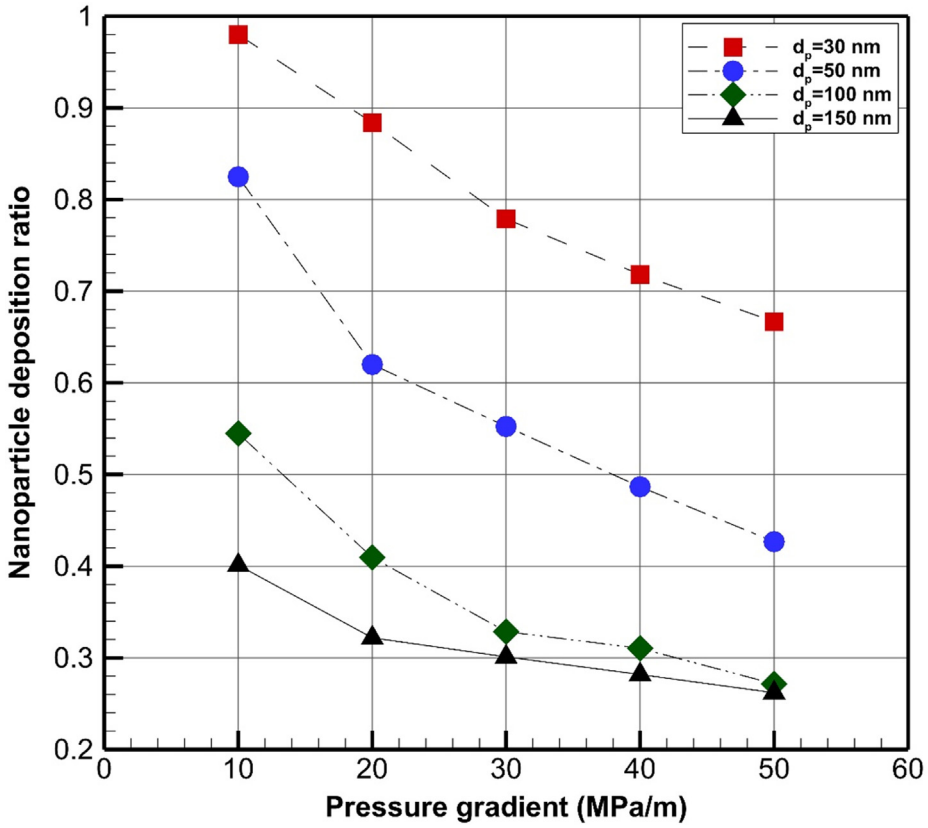

Fig. 6. The effect of pressure gradient on the nanoparticle deposition ratio for different values of nanoparticle diameter.

shows the ratio of the particle radius to the double layer thickness. As shown in this figure, with a rise of N_{DL}, the nanoparticle deposition ratio increased. For instance, when $N_{E1} = 5$, with an increase of N_{DL} from 1 to 100, the nanoparticle deposition ratio increases from 0.03 to 0.19. Also, for a constant N_{DL}, with a rise in N_{E1} value, the deposition ratio decreases. For instance, whenN_{DL} = 50, with an increase of N_{E1} from 5 to 150, the nanoparticle deposition ratio drops from 0.18 to 0.049. As N_{E1} increases, the magnitude of surface potential increases, leading to a rise in the repulsion force between nanoparticles and microchannel surfaces, which this result is also compatible with the published data in the literature [67]. But, with the rise of N_{DL} when the nanoparticle radius remains constant, the diffuse double layer around the nanoparticle and the surface of microchannels get compressed, which reduces the repulsive force and thus increases the nanoparticle deposition ratio.

Transport and deposition of nanoparticles with the 30 nm diameter and different values of N_{E1} in the microchannel are shown in Fig. 9 and Fig. 10. The size of the nanoparticles is magnified 7 times, and the results are displayed at the microchannel inlet after 0.001 s. As shown in these figures, the deposited nanoparticles on the microchannel surfaces are much higher for the nanofluid with $N_{E1} = 5$ compared to the nanofluid with $N_{E1} = 150$. The deposition ratio for $N_{E1} = 5$, is 0.094 and for $N_{E1} = 150$ is approximately 0.01.

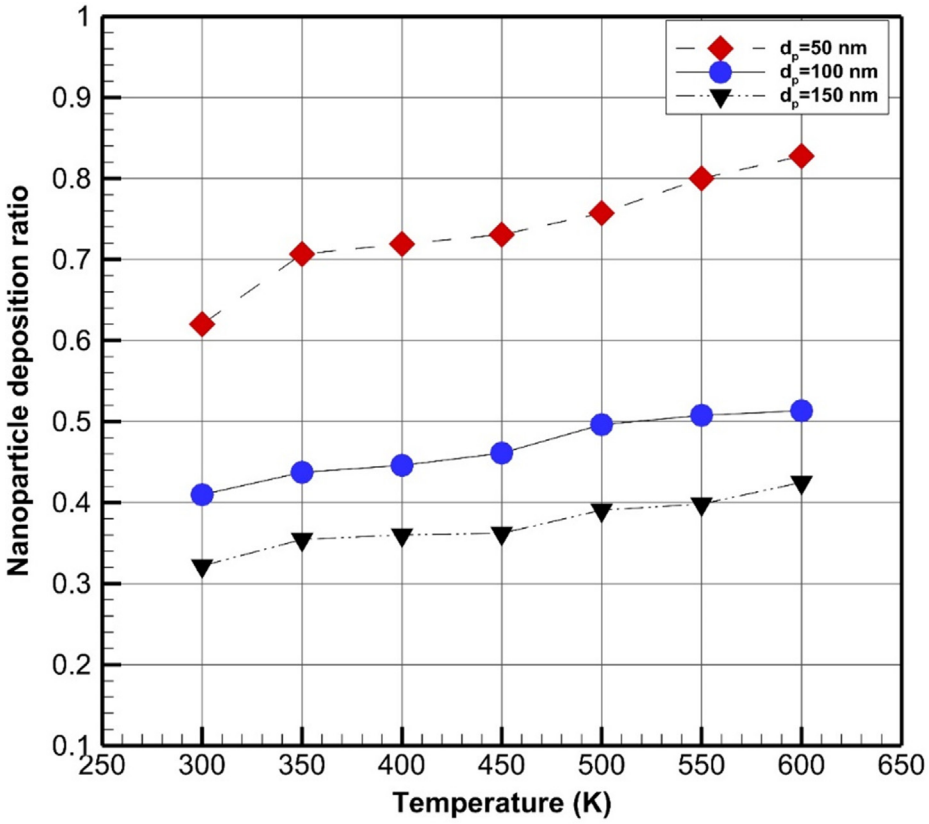

Fig. 7. Effect of temperature on the nanoparticle deposition ratio for different values of nanoparticle diameter.

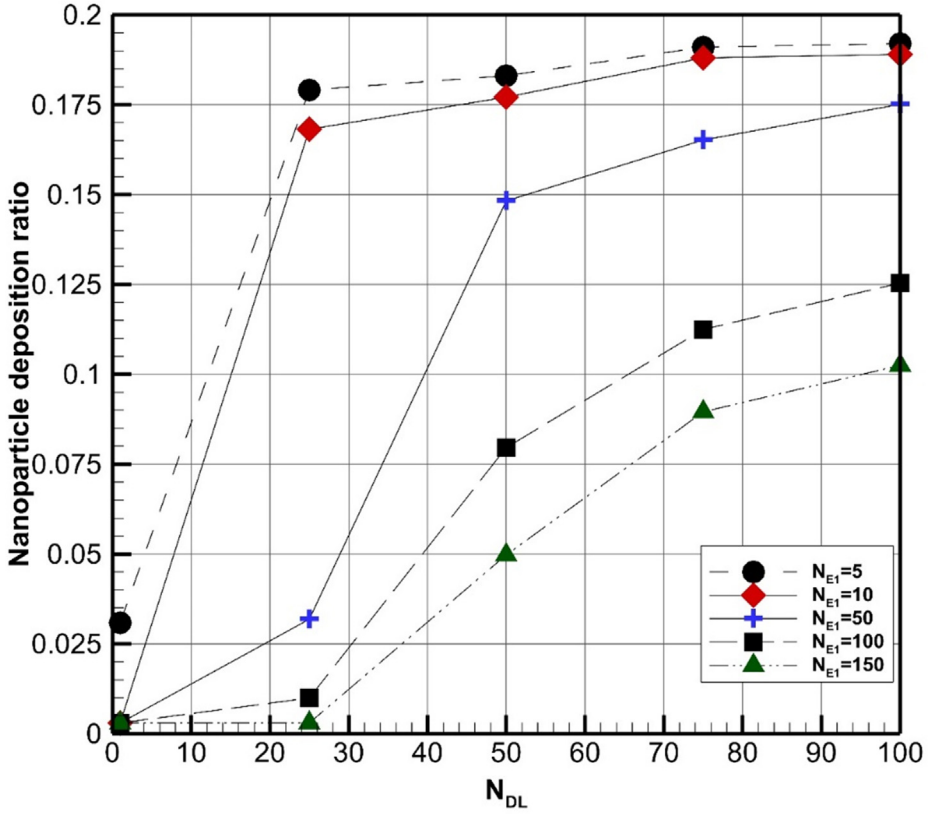

Fig. 8. The effect of N_{E1} on the nanoparticle deposition ratio for different values of N_{DL}.

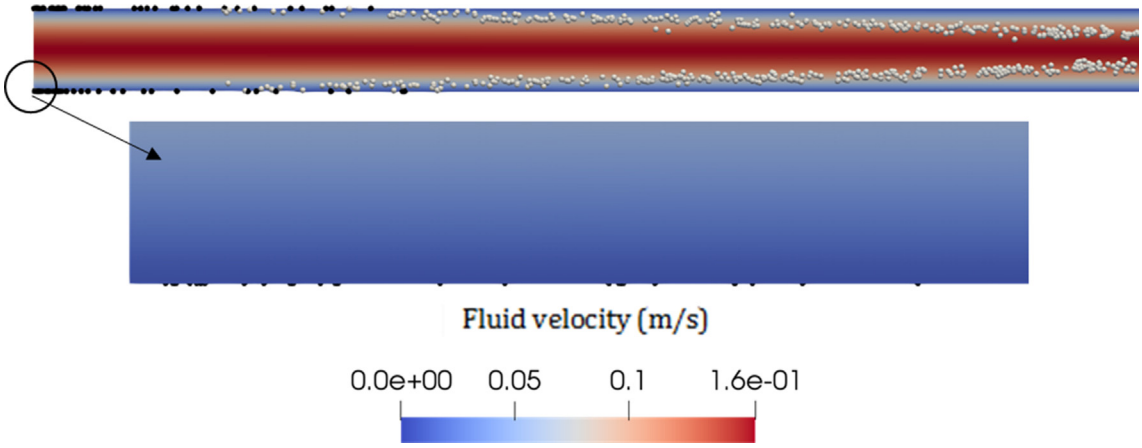

Fig. 9. Transport & deposition of nanoparticles with d_p = 30 nm, N_{E1} = 5, and N_{DL} = 50 at t = 0.001 s (black nanoparticles are deposited on the surfaces).

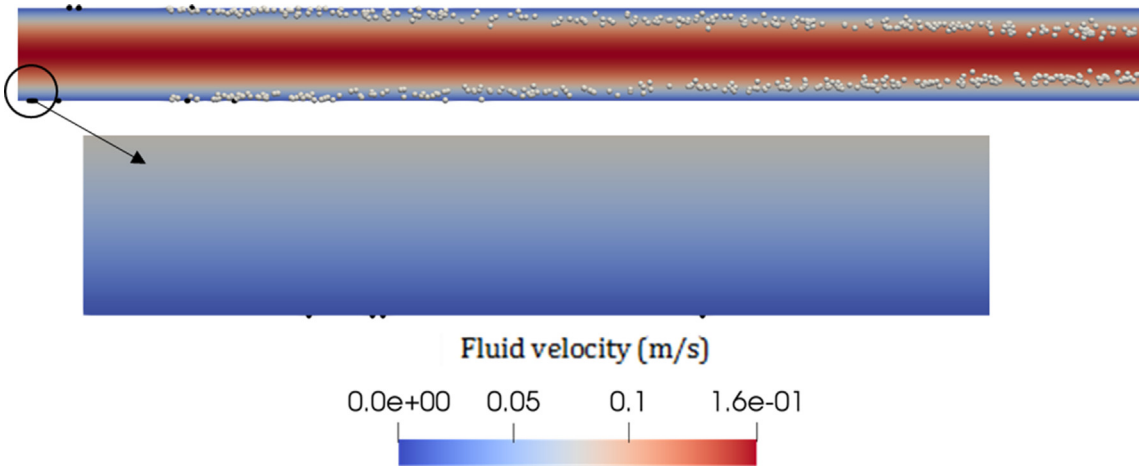

Fig. 10. Transport & deposition of nanoparticles with d_p = 30 nm, N_{E1} = 150, and N_{DL} = 50 at t = 0.001 s (black nanoparticles are deposited on the surfaces).

In Fig. 11, the effect of Re number on deposition in water, considering the effect of the EDL force, is investigated. It is assumed that the nanoparticle radius is 15 nm. An increase in velocity and consequently the Peclet number leads to superior advective transport relative to diffusive transport, which reduces the nanoparticle deposition ratio. In this figure, for three values of Re number (Re = 1, 5, and 10) and two values of N_{E1} ($N_{E1} = 10$ and 50), the nanoparticle deposition ratio as a function of N_{DL} is calculated. The maximum value of nanoparticle deposition ratio between all circumstances is for $N_{E1} = 10$ and Re = 1, and the minimum value is for $N_{E1} = 50$ and Re = 10. For $N_{DL} = 50$ and $N_{E1} = 10$, the nanoparticle deposition ratio for Re = 1, 5, and 10 are respectively 0.177, 0.0945 and 0.0756.

The nanoparticle deposition ratio for different values of nanoparticle diameter is depicted in Fig. 12. For three values of nanoparticle diameter (d_p = 30, 60, and 100 nm), nanoparticle deposition ratio as a function of N_{E1} is calculated. With an increase of nanoparticle diameter, Brownian motion decreases, leading to a decrease in deposition ratio. ForN_{E1} = 10, $N_{E2} = 1$ and $N_{DL} = 25$, the nanoparticle deposition ratio for nanoparticle diameters of 30, 60, and 100 nm are respectively 0.168, 0.133 and 0.0716.

3.4. Discussion

In this section, the data trends are compared to experimental and numerical studies on particle deposition in the literature. N_{E1}, as a non-dimensional parameter, shows the magnitude of the nanoparticle and surface potentials. With increased surface potential, the EDL repulsive force between particles and surfaces increases, decreasing particle deposition. Hence, ψ_1 and ψ_2 defining the surface potentials have a direct effect on deposition. In an experimental study, Sadeghi et al. [67] evaluated the effect of surface potentials on the deposition of virus particles in porous media, considering the variation of pH of the solution. They concluded that an increase in surface potential increases deposition. In a numerical study by Seetha et al. [47], the effect of the combined parameter ${\psi_1}^2 + {\psi_2}^2$ on the deposition of nanoparticles in a pore was studied. An increase in surface potential decreases the amount of deposition, consistent with the results of this study. The model of Seetha et al. [47] also agreed with the column experiments of Bai and Tien [68], which showed that attachment efficiency of submicron and micron-sized colloids in porous media is proportional to $({\psi_1}^2 + {\psi_2}^2)^{-0.3121}$. Also, other studies show that the trend of nanoparticle deposition by the variation of N_{E1} in this study is consistent with numerical and experimental studies in the literature [69,70]. In a study by Tufenkji and Elimelech [70], it has been shown that the attachment efficiency of colloidal particles is proportional to $({\psi_1}^2 + {\psi_2}^2)^{-1.19}$. While in the study by Seetha et al. [47] the nanoparticle attachment efficiency was proportional to $({\psi_1}^2 + {\psi_2}^2)^{-n}$, where n for different conditions had values from 0.084 to 0.762. As stated in Eq. (18), $N_{E1} \propto ({\psi_1}^2 + {\psi_2}^2)$; hence in

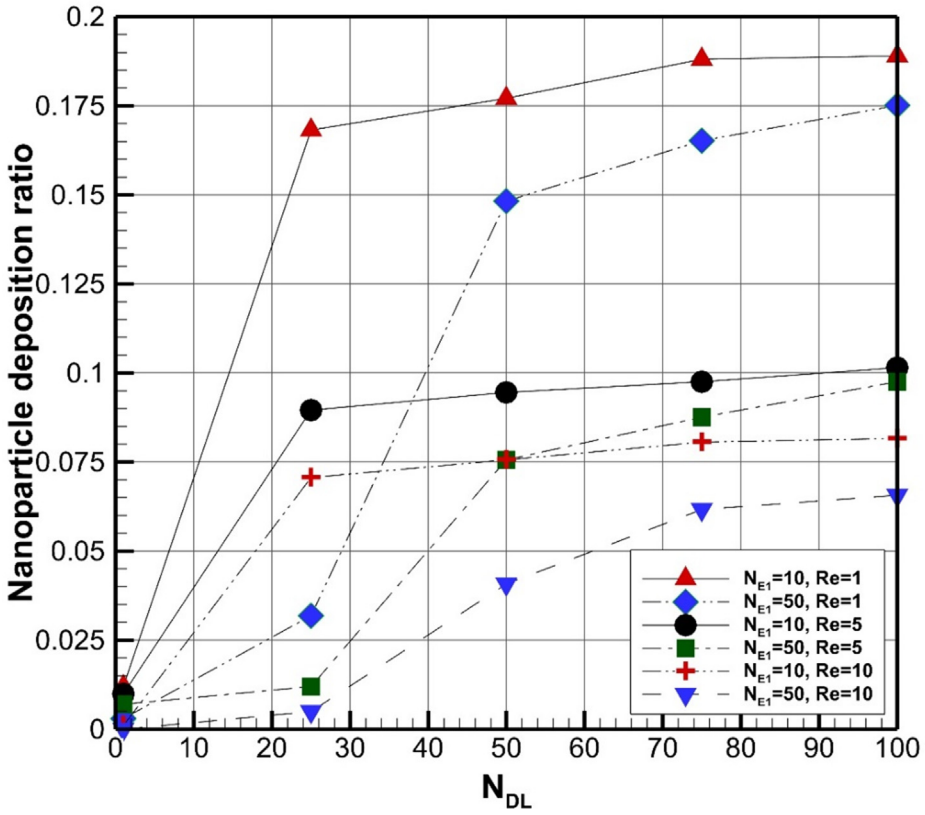

Fig. 11. The effect of N_{E1} and Re on the nanoparticle deposition ratio for different values of N_{DL} which is the ratio of the particle radius to the double layer thickness.

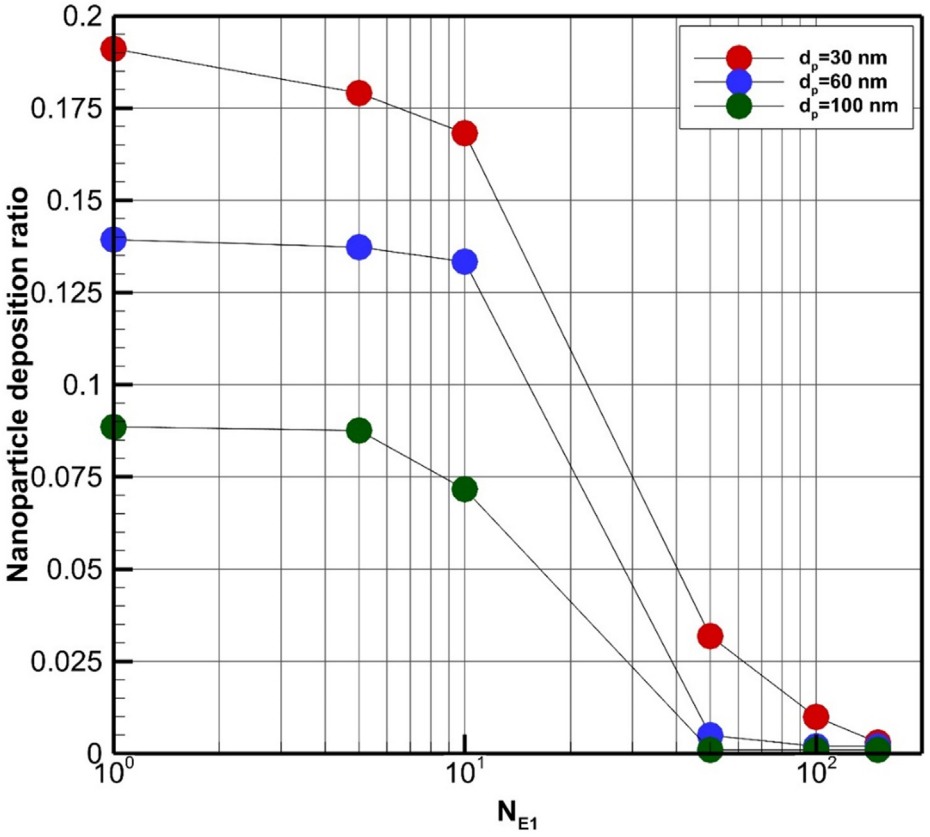

Fig. 12. The effect of nanoparticle diameter on the nanoparticle deposition ratio for different values of N_{E1}.

this study consistent to numerical and experimental studies in the literature, by the increase of N_{E1} from 1 to 10 for $N_{DL} = 25$, the nanoparticle deposition ratio decreases from 0.19 to 0.168. Also, by the increase of N_{E1} to 150, the nanoparticle deposition ratio leads to about 0.003.

Evaluation of the effects of N_{DL} on particle deposition is also of interest in the literature. As mentioned earlier, N_{DL} is a dimensionless parameter which is the particle radius divided by the Debye-Huckel length, which in turn is related to the ionic strength of the solution. With an increase of ionic strength, the electric double layers around the particle and the surfaces shrink, decreasing the EDL force and increasing particle deposition. In this simulation, it has been shown that the increase of N_{DL} can enhance the attachment efficiency of nanoparticles for different conditions from 0.01 to about 0.19. In an experimental study, Compere et al. [71] investigated the effect of solution ionic strength on the deposition of clay particles. Their conclusion on the impact of solution ionic strength on particle deposition was compatible with the results of this study. Also, in the proposed correlation equation by Bai and Tien [68], it was shown that the colloid attachment rate coefficient at Darcy-scale is proportional to solution ionic strength by the power of 0.676, which shows that this study is qualitatively consistent with the published data in the literature.

In a column experiment by Wang et al. [72], the retention and transport of silica nanoparticles in porous media were investigated. Deposition of nanoparticles 8 nm in diameter was higher than that of nanoparticles with 52 nm diameter. This fact is also compatible with correlation equations in the literature [47,68]. In this study, it has been predicted that the amount of deposition decreases with particle diameter. As shown in this study, the diffusive flux to the surfaces decreases by increasing the average flow velocity. Therefore, the number of deposited nanoparticles decreases. This agrees with the literature's column experimental and numerical results [47,73].

4. Conclusions and future directions

The deposition of nanoparticles to solid surfaces reduces the amount of material available in the bulk fluid. Also, the nanoparticle deposition increases the surface roughness of microchannel surfaces, affecting the volumetric flow rate of nanofluid. A numerical solver is developed and used in this study to achieve the effects of parameters that enhance nanoparticle deposition. In this study, an Euler-Lagrange (EL) approach is used to investigate the transport and deposition of nanoparticles mixed in a fluid in a microchannel to represent flow in porous media. A numerical solver using the OpenFOAM finite open-source library is developed, and the EL approach is used to simulate the nanoparticle behavior in interaction with the base fluid and microchannel surface. Brownian motion, drag, buoyancy, gravity, and Saffman lift forces are considered between nanoparticles and the base fluid. The simulation process of nanoparticle deposition on microchannel surfaces was performed in this study, considering all these forces between nanoparticles and the fluid. Also, Van der Waals (VDW) and electrostatic double layer (EDL) forces based on the DLVO theory are considered between nanoparticles and microchannel surfaces.

Brownian motion has a dominant effect on nanoparticle deposition. With an increase of nanofluid temperature, Brownian motion is more significant, leading to the rise in nanoparticle deposition rate. With a decrease of nanoparticle diameter, the deposition rate increases due to greater Brownian motion.

The attractive VDW force has a negligible effect on enhancing nanoparticle deposition, with a change of only 0.5–1.6% for different-sized nanoparticles in air. On the other hand, electrical double layer forces are important: larger nanoparticle and surface potentials lead to less deposition. The nanoparticle deposition rate increases with an increase of N_{DL} as the dimensionless ratio of the particle radius to the double layer thickness.

The methods used in this study can be the basis for future studies investigating the deposition of nanoparticles on the surface of porous media with different structures. The developed solver with some modifications can be the basis of the simulation of nanoparticle transport and deposition in two-phase fluid flow to enhance oil recovery with wettability alteration.

CRediT authorship contribution statement

Milad Ramezanpour: Methodology, Software, Validation, Investigation, Visualization, Writing – original draft. **Majid Siavashi:** Conceptualization, Resources, Investigation, Data curation, Writing – review & editing, Supervision, Project administration. **Ali Q. Raeini:** Conceptualization, Writing – review & editing, Supervision. **Martin J. Blunt:** Conceptualization, Writing – review & editing, Supervision.

Declaration of Competing Interest

The authors declare that they have no known competing financial interests or personal relationships that could have appeared to influence the work reported in this paper.

Acknowledgment

The authors are grateful for the financial support of the Iran National Science Foundation (INSF) [grant number: 8153].

References

[1] Z. Said, L.S. Sundar, A.K. Tiwari, H.M. Ali, M. Sheikholeslami, E. Bellos, H. Babar, Recent advances on the fundamental physical phenomena behind stability, dynamic motion, thermophysical properties, heat transport, applications, and challenges of nanofluids, Phys. Rep. 946 (2022) 1–94.
[2] A.T. Bell, The impact of nanoscience on heterogeneous catalysis, Science 299 (5613) (2003) 1688–1691.
[3] A.H. Pordanjani, S. Aghakhani, M. Afrand, M. Sharifpur, J.P. Meyer, H. Xu, H.M. Ali, N. Karimi, G. Cheraghian, Nanofluids: Physical phenomena, applications in thermal systems and the environment effects-a critical review, J. Cleaner Prod. 320 (2021) 128573, https://doi.org/10.1016/j.jclepro.2021.128573.
[4] F. Soltani, D. Toghraie, A. Karimipour, Experimental measurements of thermal conductivity of engine oil-based hybrid and mono nanofluids with tungsten oxide (WO3) and MWCNTs inclusions, Powder Technol. 371 (2020) 37–44.
[5] H. Kavusi, D. Toghraie, A comprehensive study of the performance of a heat pipe by using of various nanofluids, Adv. Powder Technol. 28 (11) (2017) 3074–3084.
[6] A.R. Rahmati, O.A. Akbari, A. Marzban, D. Toghraie, R. Karimi, F. Pourfattah, Simultaneous investigations the effects of non-Newtonian nanofluid flow in different volume fractions of solid nanoparticles with slip and no-slip boundary conditions, Therm. Sci. Eng. Prog. 5 (2018) 263–277.
[7] F. Abbas, H.M. Ali, T.R. Shah, H. Babar, M.M. Janjua, U. Sajjad, M. Amer, Nanofluid: Potential evaluation in automotive radiator, J. Mol. Liq. 297 (2020) 112014.
[8] S. Lu, K. Vafai, A comparative analysis of innovative microchannel heat sinks for electronic cooling, Int. Commun. Heat Mass Transfer 76 (2016) 271–284.
[9] H.M. Ali, H. Ali, H. Liaquat, H.T. Bin Maqsood, M.A. Nadir, Experimental investigation of convective heat transfer augmentation for car radiator using ZnO–water nanofluids, Energy 84 (2015) 317–324.
[10] N.T. Ravi Kumar, P. Bhramara, B.M. Addis, L.S. Sundar, M.K. Singh, A.C.M. Sousa, Heat transfer, friction factor and effectiveness analysis of Fe3O4/water nanofluid flow in a double pipe heat exchanger with return bend, Int. Commun. Heat Mass Transfer 81 (2017) 155–163.
[11] A. Behrangzade, M.M. Heyhat, The effect of using nano-silver dispersed water based nanofluid as a passive method for energy efficiency enhancement in a plate heat exchanger, Appl. Therm. Eng. 102 (2016) 311–317.
[12] M.H. Aghabozorg, A. Rashidi, S. Mohammadi, Experimental investigation of heat transfer enhancement of Fe2O3-CNT/water magnetic nanofluids under laminar, transient and turbulent flow inside a horizontal shell and tube heat exchanger, Exp. Therm Fluid Sci. 72 (2016) 182–189.
[13] W. He, D. Toghraie, A. Lotfipour, F. Pourfattah, A. Karimipour, M. Afrand, Effect of twisted-tape inserts and nanofluid on flow field and heat transfer characteristics in a tube, Int. Commun. Heat Mass Transfer 110 (2020) 104440.

[14] P. Barnoon, D. Toghraie, F. Eslami, B. Mehmandoust, Entropy generation analysis of different nanofluid flows in the space between two concentric horizontal pipes in the presence of magnetic field: single-phase and two-phase approaches, Comput. Math. Appl. 77 (2019) 662–692.
[15] M.R. Faridzadeh, D. Toghraie Semiromi, A. Niroomand, Analysis of laminar mixed convection in an inclined square lid-driven cavity with a nanofluid by using an artificial neural network, Heat Transfer Res. 45 (4) (2014) 361–390.
[16] M. Hemmat Esfe, M. Akbari, D. Toghraie Semiromi, A. Karimipour, M. Afrand, Effect of nanofluid variable properties on mixed convection flow and heat transfer in an inclined two-sided lid-driven cavity with sinusoidal heating on sidewalls, Heat Transfer Res. 45 (5) (2014) 409–432.
[17] S. Rostami, D. Toghraie, B. Shabani, N. Sina, P. Barnoon, Measurement of the thermal conductivity of MWCNT-CuO/water hybrid nanofluid using artificial neural networks (ANNs), J. Therm. Anal. Calorim. 143 (2) (2021) 1097–1105.
[18] D. Toghraie, N. Sina, N.A. Jolfaei, M. Hajian, M. Afrand, Designing an Artificial Neural Network (ANN) to predict the viscosity of Silver/Ethylene glycol nanofluid at different temperatures and volume fraction of nanoparticles, Physica A 534 (2019) 122142, https://doi.org/10.1016/j.physa:2019.122142.
[19] R. Saidur, T.C. Meng, Z. Said, M. Hasanuzzaman, A. Kamyar, Evaluation of the effect of nanofluid-based absorbers on direct solar collector, Int. J. Heat Mass Transf. 55 (21-22) (2012) 5899–5907.
[20] Z. Said, R. Saidur, N.A. Rahim, M.A. Alim, Analyses of exergy efficiency and pumping power for a conventional flat plate solar collector using SWCNTs based nanofluid, Energy Build. 78 (2014) 1–9.
[21] N. Akram, E. Montazer, S. Kazi, M.E.M. Soudagar, W. Ahmed, M.N.M. Zubir, A. Afzal, M.R. Muhammad, H.M. Ali, F.P.G. Márquez, Experimental investigations of the performance of a flat-plate solar collector using carbon and metal oxides based nanofluids, Energy. 227 (2021) 120452.
[22] M. Siavashi, M.V. Bozorg, M.H. Toosi, A numerical analysis of the effects of nanofluid and porous media utilization on the performance of parabolic trough solar collectors, Sustain. Energy Technol. Assess. 45 (2021) 101179.
[23] M. Siavashi, K. Ghasemi, R. Yousofvand, S. Derakhshan, Computational analysis of SWCNH nanofluid-based direct absorption solar collector with a metal sheet, Sol. Energy 170 (2018) 252–262.
[24] M. Bhatti, M. Arain, A. Zeeshan, R. Ellahi, M. Doranehgard, Swimming of Gyrotactic Microorganism in MHD Williamson nanofluid flow between rotating circular plates embedded in porous medium: Application of thermal energy storage, J. Storage Mater. 45 (2022) 103511.
[25] L. Zhang, M. Bhatti, E.E. Michaelides, M. Marin, R. Ellahi, Hybrid nanofluid flow towards an elastic surface with tantalum and nickel nanoparticles, under the influence of an induced magnetic field, European Phys. J. Special Topics. (2021) 1–13.
[26] L. Zhang, M.M. Bhatti, A. Shahid, R. Ellahi, O.A. Bég, S.M. Sait, Nonlinear nanofluid fluid flow under the consequences of Lorentz forces and Arrhenius kinetics through a permeable surface: A robust spectral approach, J. Taiwan Inst. Chem. Eng. 124 (2021) 98–105.
[27] Z. Li, P. Barnoon, D. Toghraie, R. Balali Dehkordi, M. Afrand, Mixed convection of non-Newtonian nanofluid in an H-shaped cavity with cooler and heater cylinders filled by a porous material: Two phase approach, Adv. Powder Technol. 30 (11) (2019) 2666–2685.
[28] A. Ghahremannezhad, K. Vafai, Thermal and hydraulic performance enhancement of microchannel heat sinks utilizing porous substrates, Int. J. Heat Mass Transf. 122 (2018) 1313–1326.
[29] G. Cheraghian, S. Rostami, M. Afrand, Nanotechnology in enhanced oil recovery, Processes 8 (2020) 1073.
[30] M.H. Esfe, S. Esfandeh, E. Hosseinizadeh, Nanofluid flooding in a randomized heterogeneous porous media and investigating the effect of capillary pressure and diffusion on oil recovery factor, J. Mol. Liq. 320 (2020) 113646.
[31] S. Mobaraki, M. Zakavi, O. Mahmoodi, M. Omidvar Sorkhabadi, S.S. Khalilinezhad, R. Shiri Torkmani, Shiri Torkmani, An experimental study on the mechanisms of enhancing oil recovery by nanoparticles-assisted surfactant flood, Geosyst. Eng. 23 (6) (2020) 315–331.
[32] X. Zhong, J. Chen, R. An, K. Li, M. Chen, A state-of-the-art review of nanoparticle applications with a focus on heavy oil viscosity reduction, J. Mol. Liq. 344 (2021) 117845.
[33] J. Foroozesh, S. Kumar, Nanoparticles behaviors in porous media: application to enhanced oil recovery, J. Mol. Liq. 316 (2020) 113876, https://doi.org/10.1016/j.molliq.2020.113876.
[34] B. Zhang, A.I. Mohamed, L. Goual, M. Piri, Pore-scale experimental investigation of oil recovery enhancement in oil-wet carbonates using carbonaceous nanofluids, Sci. Rep. 10 (2020) 1–16.
[35] M. Iasiello, K. Vafai, A. Andreozzi, N. Bianco, Hypo-and hyperthermia effects on LDL deposition in a curved artery, Comput. Therm. Sci. Int. J. 11 (1-2) (2019) 95–103.
[36] I.L. Molnar, P.C. Sanematsu, J.I. Gerhard, C.S. Willson, D.M. O'Carroll, Quantified pore-scale nanoparticle transport in porous media and the implications for colloid filtration theory, Langmuir 32 (31) (2016) 7841–7853.
[37] I.L. Molnar, W.P. Johnson, J.I. Gerhard, C.S. Willson, D.M. O'Carroll, Predicting colloid transport through saturated porous media: A critical review, Water Resour. Res. 51 (9) (2015) 6804–6845.
[38] J. Chatterjee, S.K. Gupta, An agglomeration-based model for colloid filtration, Environ. Sci. Technol. 43 (10) (2009) 3694–3699.
[39] I.L. Molnar, J.I. Gerhard, C.S. Willson, D.M. O'Carroll, The impact of immobile zones on the transport and retention of nanoparticles in porous media, Water Resour. Res. 51 (11) (2015) 8973–8994.
[40] O. Mahian, L. Kolsi, M. Amani, P. Estellé, G. Ahmadi, C. Kleinstreuer, J.S. Marshall, M. Siavashi, R.A. Taylor, H. Niazmand, S. Wongwises, T. Hayat, A. Kolanjiyil, A. Kasaeian, I. Pop, Recent advances in modeling and simulation of nanofluid flows-Part I: Fundamentals and theory, Phys. Rep. 790 (2019) 1–48.
[41] M. Rahimi-Gorji, O. Pourmehran, M. Gorji-Bandpy, T.B. Gorji, CFD simulation of airflow behavior and particle transport and deposition in different breathing conditions through the realistic model of human airways, J. Mol. Liq. 209 (2015) 121–133.
[42] S. Ghafouri, M. Alizadeh, S.M. Seyyedi, H. Hassanzadeh Afrouzi, D.D. Ganji, Deposition and dispersion of aerosols over triangular cylinders in a two-dimensional channel; effect of cylinder location and arrangement, J. Mol. Liq. 206 (2015) 228–238.
[43] A. Malvandi, M. Zamani, S.J. Hosseini, S.A. Moshizi, Figure of merit for optimization of nanofluid flow in circular microchannel by adapting nanoparticle migration, Appl. Therm. Eng. 118 (2017) 328–338.
[44] J. Buongiorno, Convective transport in nanofluids, J. Heat Transfer 128 (2006) 240–250.
[45] A. Malvandi, D.D. Ganji, I. Pop, Laminar filmwise condensation of nanofluids over a vertical plate considering nanoparticles migration, Appl. Therm. Eng. 100 (2016) 979–986.
[46] H. Fazeli, S. Madani, P. Rahim Mashaei, Nanofluid forced convection in entrance region of a baffled channel considering nanoparticle migration, Appl. Therm. Eng. 106 (2016) 293–306.
[47] N. Seetha, S. Majid Hassanizadeh, M.S. Mohan Kumar, A. Raoof, Correlation equations for average deposition rate coefficients of nanoparticles in a cylindrical pore, Water Resour. Res. 51 (10) (2015) 8034–8059.
[48] S.M.M. Nayinian, M. Shams, H. Afshar, G. Ahmadi, Two phase analysis of heat transfer and dispersion of nano particles in a microchannel, in (2008) 457–463.
[49] H. Afshar, M. Shams, S.M.M. Nainian, G. Ahmadi, Microchannel heat transfer and dispersion of nanoparticles in slip flow regime with constant heat flux, Int. Commun. Heat Mass Transfer 36 (10) (2009) 1060–1066.
[50] S. Andarwa, H. Basirat Tabrizi, G. Ahmadi, Effect of correcting near-wall forces on nanoparticle transport in a microchannel, Particuology. 16 (2014) 84–90.
[51] S. Andarwa, H.B. Tabrizi, Nanoparticle deposition in transient gaseous microchannel flow considering hindered motion and rarefaction effect, Korean J. Chem. Eng. 34 (5) (2017) 1319–1327.
[52] A. Albojamal, K. Vafai, Analysis of particle deposition of nanofluid flow through porous media, Int. J. Heat Mass Transf. 161 (2020) 120227.
[53] J.H. Kim, G.W. Mulholland, S.R. Kukuck, D.Y. Pui, Slip correction measurements of certified PSL nanoparticles using a nanometer differential mobility analyzer (nano-DMA) for Knudsen number from 0.5 to 83, J. Res. Nat. Inst. Stand. Technol. 110 (2005) 31.
[54] A. Li, G. Ahmadi, Dispersion and deposition of spherical particles from point sources in a turbulent channel flow, Aerosol Sci. Technol. 16 (4) (1992) 209–226.
[55] O. Abouali, A. Nikbakht, G. Ahmadi, S. Saadabadi, Three-dimensional simulation of Brownian motion of nano-particles in aerodynamic lenses, Aerosol Sci. Technol. 43 (3) (2009) 205–215.
[56] I.S. Akhatov, J.M. Hoey, O.F. Swenson, D.L. Schulz, Aerosol focusing in micro-capillaries: Theory and experiment, J. Aerosol Sci. 39 (8) (2008) 691–709.
[57] P.G. Saffman, The lift on a small sphere in a slow shear flow, J. Fluid Mech. 22 (2) (1965) 385–400.
[58] P. Saffman, Corrigendum to'The lift on a small sphere in a slow shear flow', J. Fluid Mech. 31 (1968) 624.
[59] M. Elimelech, J. Gregory, X. Jia, Particle deposition and aggregation: measurement, modelling and simulation, Butterworth-Heinemann, 2013.
[60] H.-J. Butt, M. Kappl, Surface and interfacial forces, John Wiley & Sons, 2018.
[61] J.N. Israelachvili, Intermolecular and surface forces, Academic press, 2015.
[62] P. Huang, J.S. Guasto, K.S. Breuer, The effects of hindered mobility and depletion of particles in near-wall shear flows and the implications for nanovelocimetry, J. Fluid Mech. 637 (2009) 241–265.
[63] R. Hogg, T.W. Healy, D.W. Fuerstenau, Mutual coagulation of colloidal dispersions, Trans. Faraday Soc. 62 (1966) 1638–1651.
[64] R. Rajagopalan, J.S. Kim, Adsorption of brownian particles in the presence of potential barriers: effect of different modes of double-layer interaction, J. Colloid Interface Sci. 83 (2) (1981) 428–448, https://doi.org/10.1016/0021-9797(81)90339-8.
[65] C. Fernandes, D. Semyonov, L. Ferrás, J.M. Nóbrega, Validation of the CFD-DPM solver DPMFoam in OpenFOAM® through analytical, numerical and experimental comparisons, Granular Matter 20 (2018) 1–18.
[66] H. Ounis, G. Ahmadi, J.B. McLaughlin, Brownian particle deposition in a directly simulated turbulent channel flow, Physics of Fluids A, Fluid Dyn. 5 (1993) 1427–1432.
[67] G. Sadeghi, J.F. Schijven, T. Behrends, S.M. Hassanizadeh, J. Gerritse, P.J. Kleingeld, Systematic study of effects of pH and ionic strength on attachment of phage PRD1, Groundwater 49 (1) (2011) 12–19.
[68] R. Bai, C. Tien, Particle deposition under unfavorable surface interactions, J. Colloid Interface Sci. 218 (2) (1999) 488–499.
[69] M. Elimelech, Predicting collision efficiencies of colloidal particles in porous media, Water Res. 26 (1) (1992) 1–8.
[70] N. Tufenkji, M. Elimelech, Correlation equation for predicting single-collector efficiency in physicochemical filtration in saturated porous media, Environ. Sci. Technol. 38 (2) (2004) 529–536.

[71] F. Compère, G. Porel, F. Delay, Transport and retention of clay particles in saturated porous media. Influence of ionic strength and pore velocity, J. Contam. Hydrol. 49 (1-2) (2001) 1–21.
[72] C. Wang, A.D. Bobba, R. Attinti, C. Shen, V. Lazouskaya, L.-P. Wang, Y. Jin, Retention and transport of silica nanoparticles in saturated porous media: effect of concentration and particle size, Environ. Sci. Technol. 46 (2012) 7151–7158.
[73] X. Li, P. Zhang, C.L. Lin, W.P. Johnson, Role of hydrodynamic drag on microsphere deposition and re-entrainment in porous media under unfavorable conditions, Environ. Sci. Technol. 39 (11) (2005) 4012–4020.